ORIGINAL ARTICLE

Repurposing sarecycline for osteoinductive therapies: an in vitro and ex vivo assessment

Victor Martin[1,2] · Liliana Grenho[1,2] · Maria H. Fernandes[1,2] · Pedro S. Gomes[1,2]

Abstract

Introduction Tetracyclines (TCs) embrace a class of broad-spectrum antibiotics with unrelated effects at sub-antimicrobial levels, including an effective anti-inflammatory activity and stimulation of osteogenesis, allowing their repurposing for different clinical applications. Recently, sarecycline (SA)—a new-generation molecule with a narrower antimicrobial spectrum—was clinically approved due to its anti-inflammatory profile and reduced adverse effects verified with prolonged use. Notwithstanding, little is known about its osteogenic potential, previously verified for early generation TCs.

Materials and Methods Accordingly, the present study is focused on the assessment of the response of human bone marrow-derived mesenchymal stromal cells (hBMSCs) to a concentration range of SA, addressing the metabolic activity, morphology and osteoblastic differentiation capability, further detailing the modulation of Wnt, Hedgehog, and Notch signaling pathways. In addition, an ex vivo organotypic bone development system was established in the presence of SA and characterized by microtomographic and histochemical analysis.

Results hBMSCs cultured with SA presented a significantly increased metabolic activity compared to control, with an indistinguishable cell morphology. Moreover, RUNX2 expression was upregulated 2.5-fold, and ALP expression was increased around sevenfold in the presence of SA. Further, GLI2 expression was significantly upregulated, while HEY1 and HNF1A were downregulated, substantiating Hedgehog and Notch signaling pathways' modulation. The ex vivo model developed in the presence of SA presented a significantly enhanced collagen deposition, extended migration areas of osteogenesis, and an increased bone mineral content, substantiating an increased osteogenic development.

Conclusion Summarizing, SA is a promising candidate for drug repurposing within therapies envisaging the enhancement of bone healing/regeneration.

Keywords Sarecycline · Bone tissue · In vitro · Ex vivo · Drug repurposing

Introduction

Tetracyclines (TCs) embrace a class of broad-spectrum bacteriostatic antibiotics that inhibit the bacterial protein synthesis by binding to the 30S ribosomal subunit, being effective against a wide range of bacteria, including aerobic, anaerobic, Gram-positive, and Gram-negative pathobionts [1].

Of additional relevance, non-antimicrobial effects of TCs with potential clinical application were described, including anti-inflammatory properties, inhibition of matrix metalloproteinases (MMPs), and stimulation of osteogenesis, found to be effective at sub-antimicrobial concentrations [2]. This opened a window of opportunity for their repurposing, leading to their clinical application for different indications, as dermatoses, diabetes-related

✉ Pedro S. Gomes
 pgomes@fmd.up.pt

 Victor Martin
 vmartin@fmd.up.pt

 Liliana Grenho
 lgrenho@fmd.up.pt

 Maria H. Fernandes
 mhfernandes@fmd.up.pt

[1] LAQV/REQUIMTE, U. Porto, 4160-007 Porto, Portugal

[2] BoneLab - Laboratory for Bone Metabolism and Regeneration - Faculty of Dental Medicine, U. Porto, Rua Dr. Manuel Pereira da Silva, 4200-393 Porto, Portugal

complications, periodontal disease, rheumatoid arthritis, bowel disease, Parkinson's disease, and enhanced bone healing, among others [2, 3].

Regarding the osteogenic capability of TCs, controversial results can be found in the literature. For instance, some in vitro studies reported that low TC concentrations induce the osteoblastic proliferation rate, enhance alkaline phosphatase (ALP) activity and calcium deposition, and upregulate the osteogenic gene program, without impairing phenotypic or functional activity [4, 5]. However, other studies reported no increase in cell proliferation neither any induction of the osteogenic program by low TCs' concentrations [6, 7]. Nevertheless, using in vivo models, either independently or conjugated with different bone-related biomaterials, studies tend to report overall positive results. In addition, substantial outcomes in clinical trials were obtained by the conjugation of TCs with biomaterials targeting bone healing in periodontal disease [8].

Most recently, a new generation of synthetic TCs (e.g., tigecycline, eravacycline, and omadacycline) has been developed, with its use largely restricted to community-acquired bacterial pneumonia and intra-abdominal infections, due to their retained activity against tetracycline-resistant organisms as methicillin-resistant *Staphylococcus aureus* [9]. Additionally, Sarecycline (SA), also a new-generation molecule with a narrower spectrum of antimicrobial activity, has been approved for acne vulgaris' treatment, due to its anti-inflammatory profile and absence of adverse side-effects associated with prolonged administrations—as gastrointestinal disorders, mycotic infections, and increased potential of bacterial resistance [10, 11].

SA antimicrobial profile was already characterized in vitro and in vivo—SA presents a similar activity against Gram-positive bacteria, being much less effective against Gram-negative bacteria, when compared to early generation TCs [11]. Further, SA demonstrated a comparable anti-inflammatory activity within an in vivo paw edema model, further presenting a significant reduction of inflammatory acne lesions in clinical trials [12]. However, little is known about SA osteogenic potential, as to the best of the authors' knowledge, the effects of SA on bone tissue or related cell populations have not been addressed previously, either in vitro, ex vivo, or in vivo.

Accordingly, the present study is focused on the assessment of the in vitro response of osteoblastic-precursor cells to SA, at different concentrations, addressing distinct functional parameters as metabolic activity, morphology, and osteoblastic differentiation at the molecular level, further uncovering the potential modulation of Wnt, Hedgehog, and Notch signaling pathways. In addition, to provide an in-depth analysis of the bone tissue to this new-generation TC, an ex vivo femoral organotypic system was further established, developed, and characterized in the presence of SA.

Materials and methods

Materials

α-MEM culture medium, fetal bovine serum (FBS), penicillin, streptomycin, amphotericin-B and TrypLE (all Gibco); Tetrazolium salt (3-(4,5-dimethylthiazol-2-yl)-2,5-diphenyltetrazolium bromide) (MTT kit, Sigma-Aldrich), Triton-X, p-nitrophenyl phosphate (ALP kit, Sigma-Aldrich), Albumin Bovine, Alcian blue/Sirius red/von Kossa reagents (all Sigma-Aldrich); iTaq Universal SYBR green Supermix PCR Kit and primers (all Bio-Rad), Trizol reagent (Ambion Life technologies), NZY first-strand cDNA synthesis kit (NZY-TECH), phalloidin-conjugated Alexa Fluor 488 (Molecular Probes), MitoSpy™ Red FM (Biolegend), Hoechst 33342 (Enzo), and Quant-iT™ PicoGreen® ds-DNA kit (Invitrogen). Sarecycline hydrochloride (SA) was kindly donate by Adooq Bioscience.

In vitro assessment of sarecycline osteogenic potential: osteoblastic cell cultures

Sarecycline activity was characterized in vitro using human bone marrow-derived mesenchymal stromal cells (hBMSCs—Human Mesenchymal Stem Cells, Lonza, Catalog #: PT-2501). Cells were characterized by flow cytometry and found to be positive for CD105, CD73, and CD90, and negative for CD45, CD34, and CD14 markers. Cells from the 4th passage were used in the present experiment. hBMSCs' cultures were expanded in α-MEM culture medium, containing 10% FBS, 100 IU/mL penicillin, 100 μg/mL streptomycin, and 2.5 μg/mL amphotericin-B, and were incubated at 37 °C and 5% CO_2. At a confluence of approximately 70%, grown cells were detached and sub-cultured at 10^4 cells/cm². After 24 h, cultures were incubated with complete culture medium supplemented with 10% SA solutions (V/V), reaching final concentrations of 0.1, 1 and 10 μg/mL, in accordance with experimental conditions. For the gene expression and ALP activity analysis, hBMSCs cultures were incubated with SA at 1 μg/mL. Cultures grown in complete culture media devoid of SA were used as basal control condition (C-BAS).

Metabolic activity and DNA content

Metabolic activity of the cell cultures was determined by MTT assay. At selected time-points, MTT solution (5 mg/mL) was added and cultures were incubated for 3 h. Following, the supernatant was removed, crystals were dissolved with dimethyl sulfoxide, and the absorbance of the colored solution was determined at 550 nm with a microplate reader (Synergy HT; BioTek). In addition, DNA quantification was

performed as previously described [13]. Briefly, at the same selected time-points, cultures were treated with 0.1% Triton-X-100 for 15 min, and then, a Quant-iT™ PicoGreen® ds-DNA kit was employed according to the manufacturer's instructions. Fluorescence was determined at 480/520 nm (excitation/emission) using the same microplate reader. Five independent experiments were performed.

Cell morphology

Cell morphology was assessed by fluorescence microscopy, upon staining of F-actin cytoskeleton and mitochondria, using phalloidin-conjugated Alexa Fluor 488 and Mito-Spy™ Red FM, respectively, followed by a nucleus counterstaining with Hoechst 33342. Representative images were captured using a Celena S digital imaging system (Logos Biosystems). Briefly, at 24 and 120 h of culture, cells were incubated for 30 min with MitoSpy™ Red FM, at 37 °C and 5% CO_2. Cells were then fixed with paraformaldehyde 3.7%, following their permeabilization with Triton-X 0.1% and incubation with bovine serum albumin at room temperature. Finally, cells were stained with phalloidin-conjugated Alexa Fluor 488 and Hoechst 33342, for F-actin and nucleus staining, respectively, and proceeded to microscopic analysis. Images were treated using the ImageJ software v.1.53 k. Five independent experiments were performed.

Gene expression analysis

Total RNA was isolated from hBMSCs cultures grown for 7 days using Trizol reagent, in accordance with the standard manufacturer's protocol. RNA concentration and quality were assessed by absorbance reading (A260/A280) with NanoDrop (NanoDrop Technologies). Samples with A260/A280 ratio of approx. 2.0 were proceeded to cDNA conversion.

The conversion to cDNA was conducted with a reverse transcription system, normalizing the RNA' concentration to 500 ng/μL, reaching a final volume of 20 μL for each sample. Conversion' cycle was set as 10 min at 25 °C, 30 min at 50 °C, and 5 min at 85 °C. Then, 1 μL of RNAse was added to each sample prior incubation at 37 °C for 20 min.

Quantitative PCR (qPCR) was performed with a CFX384 real-time PCR system (Bio-Rad), using 5 μL of iTaq Universal SYBR green Supermix PCR Kit, 3.5 μL of DEPC water, 0.5 μL of the primer, and 1 μL of cDNA in each well. The Bio-Rad cycling protocol was applied (activation—2 min at 95 °C; 40 cycles of denaturation/annealing, 5 s at 95 °C and 30 s at 60 °C; melt curve, 65–95 °C). DEPC water was used as negative control for each primer.

Quality control was checked using Bio-Rad CFX Maestro 1.1, v.4.1.24. Samples with amplification efficiency greater than 110 and less than 90 were excluded, as well as samples with a linear standard curve (R^2) less than 0.98. The relative quantification of each target gene was normalized using the housekeeping gene (GAPDH) levels and final values were calculated via the $2^{-\Delta\Delta Ct}$ method. The references of the used primers are presented in Table 1. Five independent experiments were performed.

Alkaline phosphatase (ALP) activity

ALP activity from 14-day cultures was determined in cell lysates after the treatment with Triton-X 0.1%. Quantitative analysis was performed following the dissolution of p-nitrophenyl phosphate in an alkaline buffer solution (pH 10.3) and the colorimetric determination of the p-nitrophenol product was measured at 405 nm using a microplate reader (Synergy HT, BioTek). Hydrolysis was established for 30 min, at 37 °C. ALP levels were normalized for the levels of total protein, assayed by the method of Lowry, using a DC protein kit (Bio-Rad), and the same microplate reader, at 750 nm. Results were expressed in nanomoles of p-nitrophenol produced per min per μg of protein (nmol/min/μg protein). Five independent experiments were performed.

Ex vivo assessment of sarecycline osteogenic functionality: organotypic cultures of embryonic chick femora

The influence of SA on bone tissue development was assayed within an ex vivo model—the embryonic chick femora organotypic culture. The experimental use for research of avian fetal forms within the first two-thirds of development is not encompassed by the current European (Directive

Table 1 The assay ID of the used primers

Gene	Assay ID	Gene	Assay ID
GAPDH	qHsaCED0038674	SPARC	qHsaCID0010332
RUNX2	qHsaCED0044067	PTCH1	qHsaCEP0055042
SP7	qHsaCED0003759	GLI2	qHsaCEP0057630
COL1A1	qHsaCED0043248	HEY1	qHsaCEP0053501
BGLAP	qHsaCED0038437	HES1	qHsaCED0006922
ALP	qHsaCED0045991	AXIN2	qHsaCID0017930
BMP2	qHsaCID0015400	HNF1A	qHsaCEP0024214
TWIST1	qHsaCED0003856		

Primers were purchased from Bio-Rad

GAPDH, glyceraldehyde-3-phosphate dehydrogenase; RUNX2, runt-related transcription factor 2; SP7, Osterix; COL1A1, collagen type I alpha 1; BGLAP, Osteocalcin; ALPL, alkaline phosphatase; BMP2, bone morphogenetic protein 2; TWIST1, Twist family BHLH transcription factor 1; SPARC, Osteonectin; PTCH1, Protein Patched Homolog 1; GLI2, Glioma-Associated Oncogene Family Zinc Finger 2; HEY1, HES-Related Repressor Protein 1; HES1, Hes Family BHLH Transcription Factor 1; AXIN2, axis inhibition protein 2,; HNF1A, Hepatocyte nuclear factor 1-alpha

2010/63/EU) or National (Decreto-Lei n.º 113/2013) legislation, precluding the need for regulatory approval of the experimental procedures.

Briefly, fertilized chick eggs (*Gallus domesticus*) acquired from a certified vendor were incubated in an automatic egg incubator (Octagon Advance, Brinsea) until the 11th day of development. Then, chick embryos were euthanized and the femurs were dissected and carefully placed into Netwell® inserts (Costar 3480, 440 µm of pore diameter) in 6-well plates. Femurs were maintained for 24 h in α-MEM culture medium supplemented with ascorbic acid (50 µg/mL), penicillin (100 U/mL)/streptomycin (100 µg/mL), and 2.5 µg/mL amphotericin-B, at liquid/gas interface, in a humidified atmosphere of 5% CO_2 in air, and 37 °C. After, the medium was replaced by the previously described medium, further supplemented with SA, at 1 or 10 µg/mL. Control femurs were grown in the absence of SA, with daily changes of the culture media, for an 11-day period. Femora were following characterized by microtomographic evaluation and histochemical analysis, as following detailed.

Morphometric analysis by micro-computed tomography (µCT)

At the end of the experimental period, selected femurs were scanned at 40 kV, 100 µA, and an isotropic resolution of 4.5 µm, using a Skyscan 1276 Microtomographic System (Bruker, Belgium). The obtained projection images were reconstructed with NRecon software (Bruker, version 1.7.4.2). Morphological analysis of the bone was set on the region of interest (ROI), obtained by the separation of femur samples from the background noise and the eppendorf. The quantitative analysis was carried out in 900 slices at the diaphysis region (450 slices above and 450 below the mid-diaphysis) with CTAnalyser software (Bruker, version 1.0.11), contemplating the following parameters: bone volume (BV), bone surface (BS), and tissue volume (TV), and associated ratios BV/TV, BS/BV, and BS/TV. Three-dimensional images were generated using CTVox software (Bruker, version 3.3.0). Five independent experiments were performed.

Histochemical staining

At the end of the experimental period, selected femurs were fixed in 4% paraformaldehyde, embedded in paraffin blocks, and cut in 5 µm-thick sections. Then, sections were marked with Alcian blue/Sirius red (AB/SR) for the staining of glycosaminoglycans and collagenous matrix, respectively. In addition, femurs' sections were also stained using von Kossa's dyeing for calcified tissue visualization, relying on the replacement of calcium by silver and ultraviolet light exposure, producing dark metallic areas [14]. Images were

captured using a Zeiss Axiolab 5 microscope coupled with an Axiocam 5 Color Camera. The percentage of collagen and mineralized areas of AB/SR and von Kossa's obtained images, respectively, were calculated using ImageJ software (version 1.53 k), after setting the thresholding of images with Huang algorithm [15]. Three independent experiments were performed.

Statistical analysis

Statistical analysis and graphics were performed using the IBM SPSS v.26 software. The data normality was determined by the Shapiro–Wilk test. For normal datasets, one-way ANOVA was performed, followed by multiple comparisons using Tukey's test. For non-parametric datasets, Kruskal–Wallis test was performed, followed by multiple comparisons using Dunn's tests. p values < 0.05 were considered significant. Data were presented as mean $\pm$ standard deviation (SD).

Results

### In vitro assessment of sarecycline osteogenic functionality

In vitro hBMSCs' cultures were established and grown in the presence and absence of selected concentrations of SA. In control cultures, both MTT reduction values and total DNA content were found to increase until day 21, a trend followed by cultures grown in the presence of SA 0.1 µg/mL, found to be significant increased from day 7 onwards regarding the MTT assay (Fig. 1-A). Total DNA levels for cultures grown in the presence of SA 0.1 µg/mL were found to be significantly higher at day 14 (Fig. 1-B). Cultures grown in the presence of SA 1 and 10 µg/mL also presented a trend for higher metabolic activity up to day 14—being significantly higher than control at days 7 and 14. Similar growth curve can be observed in Fig. 1-B by the quantification of total DNA, confirming an active proliferation of hBMSCs' cultures in control and experimental groups. It is noted that SA at 1 µg/mL presented the highest DNA amount at day 14.

Regarding the assessment of cell morphology at day 1 (Fig. 2-A), hBMSCs' control cultures presented a morphologically homogeneous phenotype, with well-organized F-actin filamentous fibers, an elongated morphology, prominent nucleus, and a feeble mitochondrial staining. In addition, a polygonal morphology is observed, as an evident cytoplasmic spreading, with filopodial protrusions and spikes, extending and establishing direct contact with adjacent cells. A strong similarity is noted in cells exposed to SA, with mitochondrial staining mostly concentrating at
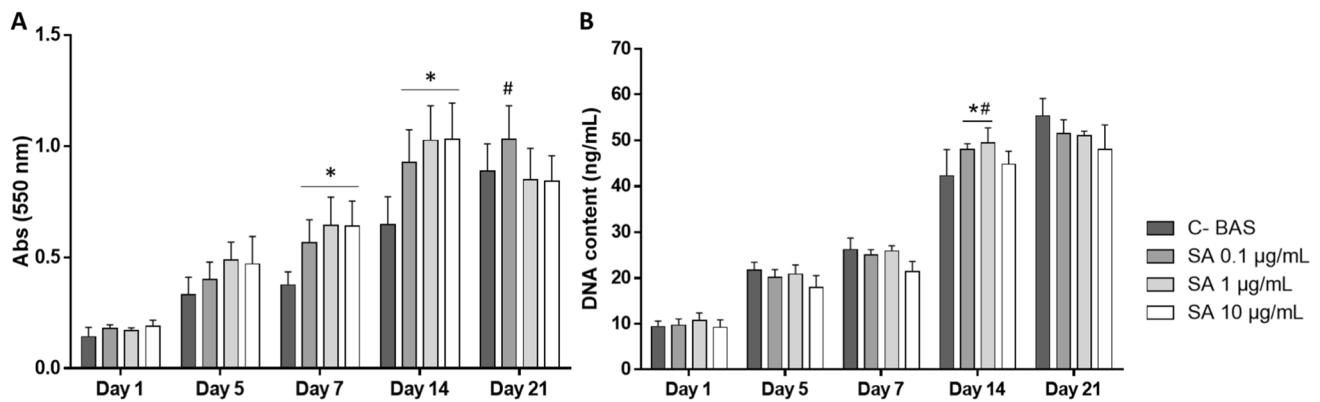
Fig. 1 **A** Metabolic activity/cell viability—MTT assay; and cell proliferation—total DNA **B** of hBMSCs cultured with different concentrations of sarecycline, up to 21 days. *Significantly different to control; #significantly different to experimental groups ($n=5$, $p<0.05$)
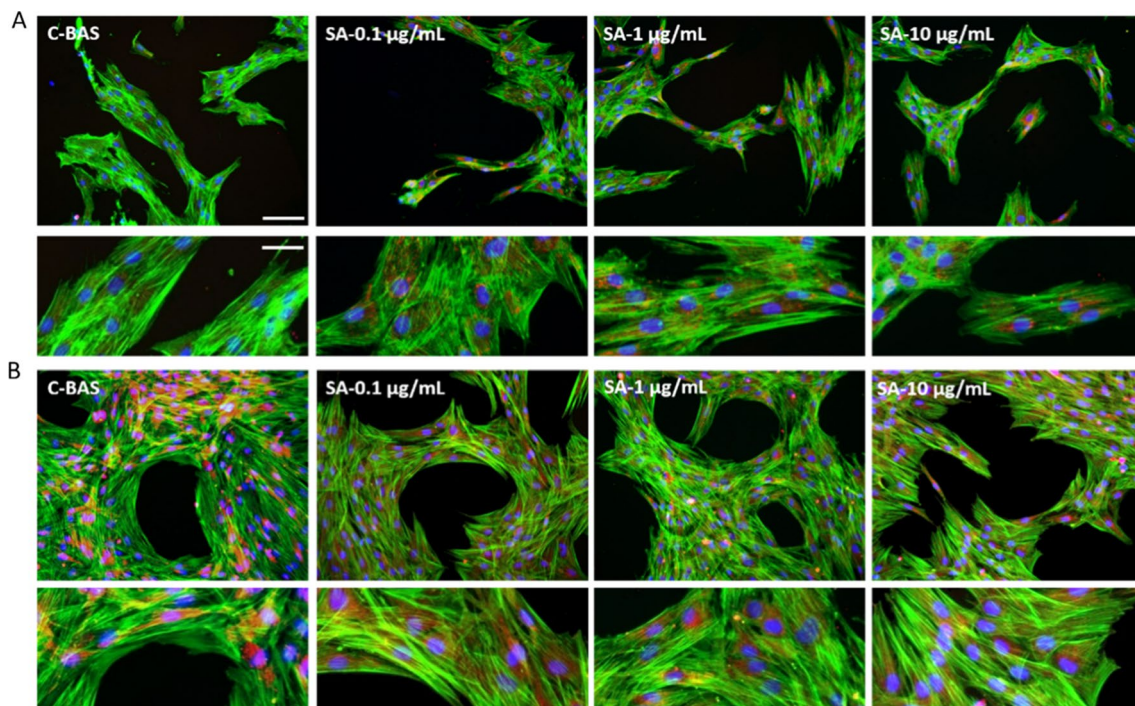
**Fig. 2** Representative fluorescent images of hBMSCs exposed to sarecycline, stained for cytoskeleton (F-actin, green) and mitochondria (red), counterstained for nucleus (blue). Images representative of 24 h (**A**) and 5 days (**B**) of culture. Scale bars correspond to 100 μm on first and third lines of figures and 25 μm on the second and fourth lines of figures, respectively. $n=5$

the perinuclear area, being suggestive of a healthy cellular functionality.

At day 5 (Fig. 2-B), hBMSCs' cultures presented a higher cellular density areas—confirming an active proliferation—with abundant intercellular contacts, as well as an increased mitochondria presence around the nucleus, for control and experimental cultures. No differences were observed between the control cultures and experimental groups.

The osteoblastic differentiation of hBMSCs was evaluated through qPCR (Figs. 3 and 4), contemplating distinct osteogenic markers and relevant osteogenic signaling pathways. hBMSCs exposed to SA presented significant differences regarding the osteogenic gene expression in comparison to control. For instance, RUNX2 was upregulated 2.5-fold and its downstream genes, COL1A1 and osteonectin (SPARC) were slightly upregulated. Importantly, ALP expression was sevenfold increased, which is

Fig. 3 **A** Relative expression of osteogenesis-related genes of hBMSCs cultured with SA at 1 µg/mL, for 7 days. Values were normalized by the gene expression values at the control culture. **B** Quantitative ALP activity of HBMSCs cultured with sarecycline at 1 µg/mL, for 14 days. *Significantly different to control ($n = 5$, $p < 0.05$)
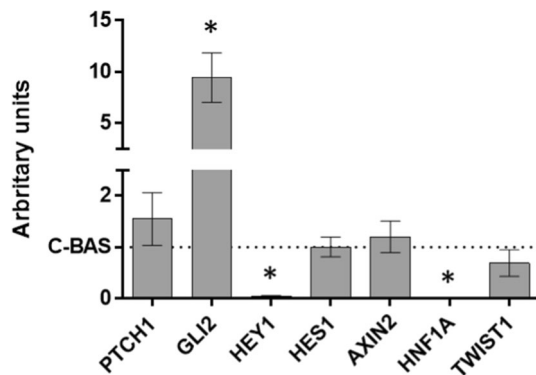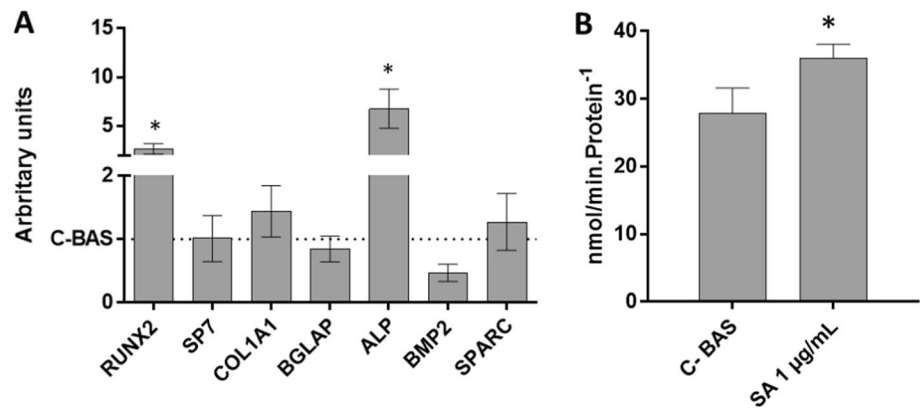
Fig. 4 Relative expression of genes associated with relevant signaling pathways (Hedgehog, Notch, and Wnt) of hBMSCs cultured with SA at 1 µg/mL, for 7 days. Values were normalized by the gene expression values at the control culture. *Significantly different to control ($n = 5$, $p < 0.05$)

supported by a significant increase of the enzyme's activity (Fig. 3-B). However, the experimental group presented some downregulation of BMP2, an important inducer of osteogenic differentiation and bone formation.

Further, the activation of relevant signaling pathways on the osteogenic differentiation—Hedgehog, Notch, and Wnt—were also assessed in the presence of SA. Hedgehog signaling was found to be stimulated, once GLI expression was significantly upregulated (9.5-fold), while PTCH1—a surface receptor that activates GLI transcription factor expression—also presented some increased expression.

Substantial changes were also verified in the gene expression of Notch signaling—HES1 was unaltered by SA's exposure; however, HEY1 was strongly downregulated by SA. Finally, the Wnt signaling was assessed by TWIST1, AXIN2, and HNF1A expression. AXIN2 and TWIST1 levels were similar to control, while HNF1A/TCF1 were massively downregulated.
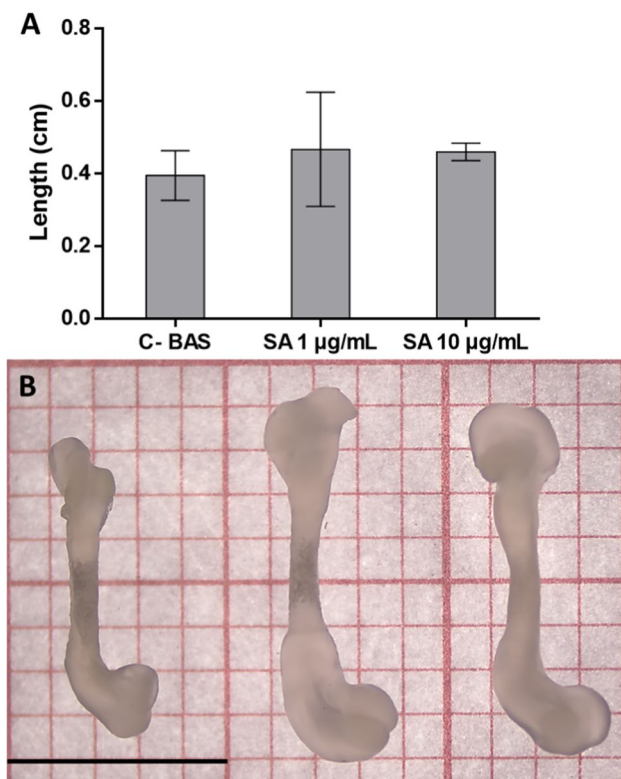
Ex vivo assessment of sarecycline osteogenic functionality: organotypic cultures of embryonic chick femora

The biological response to SA was further addressed in an ex vivo model of the embryonic chick femora development, to provide an in-depth analysis of cell differentiation, mineralization stages, and developmental growth patterns, maintaining the relationship of the cells within their extracellular matrix [16].

The first parameter analyzed was the length of the femurs exposed to two concentrations of SA, for 11 days (Fig. 5). The incubation with SA marginally increased the femurs' length in comparison to control. Moreover, femurs incubated with SA markedly enlarged the cartilage of the epiphyseal region.

Second, the bone morphometric analysis was set on the correlation of µCT results and the histological/histochemical evaluation of the corresponding femurs. µCT results showed that the addition of SA to E11 femur cultures resulted in a significant increase in mineralized content, as verified by a higher BV/TV ratio (Fig. 6-D). In addition, bone surface density (BS/TV) was found to be significantly higher in the presence of SA. Comparing experimental groups, SA at 1 µg/mL presented a stronger osteogenic potential in relation to SA at 10 µg/mL, presenting a significant increase in the BS/BV ratio, as well as in the bone surface density (BS/TV).

Regarding the histochemical analysis, the diaphysis region of control femora presented an exterior collar of collagen-rich matrix stained by Sirius red, and an interior filled with a proteoglycan-rich matrix, dyed by Alcian blue (Fig. 7-A). In addition, a mild reddish accent can be observed within the interior cartilage matrix, as well as empty spaces, suggesting some cell migration and the initiation of the trabecular organization, characteristic of the expected phenotypic development. Experimental groups presented more extended cellular migration areas within the internal diaphysis, in addition to a significant increase in collagen thickness over the marginal region for both SA concentrations, verified by

Fig. 5 **A** Variation of the bone length of the femurs grown with SA. **B** Representative macroscopic images of control, SA at 1 and 10 μg/mL, respectively. Scale bar corresponds to 5 mm ($n = 5$, $p < 0.05$). No statistical differences among groups were attained

Comparing the metabolic activity and cell proliferation of hBMSCs' cultures grown in the presence of SA (Fig. 1-A and B), with those grown in the presence of early generation TCs, it is noticeable that SA, even at higher concentrations (10 μg/mL), did not present any impairment or initial dose-dependent inhibitory effects, as previously verified, suggesting an enhanced cytocompatibility [4, 18]. For instance, in the study of Gomes and Fernandes (2007), the metabolic activity of hBMSCs cultured with doxycycline and minocycline was assessed and an initial inhibitory effect was observed even at low concentrations (1 μg/mL)—despite the improvement with longer culture times, and a significant impairment attained with higher concentrations [4]. Similar results were obtained with different cell lines, demonstrating the inhibitory effects of TCs at concentrations higher than 10 μg/mL [18, 19]. This enhancement of the metabolic activity may be related to the improvement of the status of energy coupling in mitochondria, triggered by several factors, as the possibility to modify the membrane potential, modulating the mitochondrial respiratory chain and ATP synthase activity [20]. In addition, selected second generation TCs' concentrations also seem to decrease the expression of caspases and inhibit cytochrome-c release through specific signaling of Bcl-2 and XIAP, thus modulating both the intrinsic and extrinsic apoptotic pathways into an increased cell viability [21, 22].

Regarding the morphology of hBMSCs cultures (Fig. 2), some studies associate a rounded shape with adipogenic differentiation and a slower proliferative profile, while a polygonal-shape and the presence of a high density of filopodia-like protrusions are usually correlated with an enhanced osteogenic differentiation of precursor populations [23, 24]. In addition, our findings diverge from other studies with previous generation TCs—in the study of Park (2011), osteoprecursor cells cultured with TCs presented a reduction of the number of the cells at 10 μM and a more rounded shape and reduced attachment at 100 μM [6]. A similar pattern was observed in the study of Almazin et al. [25]; primary osteoblasts cultured with minocycline presented a rounded morphology and a decreased number of the cells. Gathering the information, our results suggest that hBMSCs' cultures incubated with SA presented a morphology associated with a proliferative profile and the priming of the osteogenic activation.

The gene expression pattern of osteoblastic-related genes (Figs. 3 and 4) reported in the literature is similar to the one of the present study—RUNX2 and ALP were found to be upregulated when cells were cultured with low-dosage TCs [5, 26, 27]. RUNX2 is considered the master osteogenic transcription factor [28], while ALP is a known early osteoblastic marker, essential to catalyze the liberation of phosphate from various substrates allowing the formation of hydroxyapatite and the consequently maturation the bone

the quantification of collagen areas (Fig. 7-C). Moreover, the von Kossa staining evidenced a mineral deposition within the collagen outer layer at the mid-diaphysis (Fig. 7-B). Among samples, noticeable differences can be observed. Femurs exposed to SA presented abundant mineralized areas, with significant stronger staining, as well as thicker and more developed mineralized trabeculae, corroborated by the quantitative analysis (Fig. 7-D). In fact, the significant increase in bone volume (BV/TV) observed within μCT analysis correlates with the increased collagen and mineral deposition observed within the diaphyseal section.
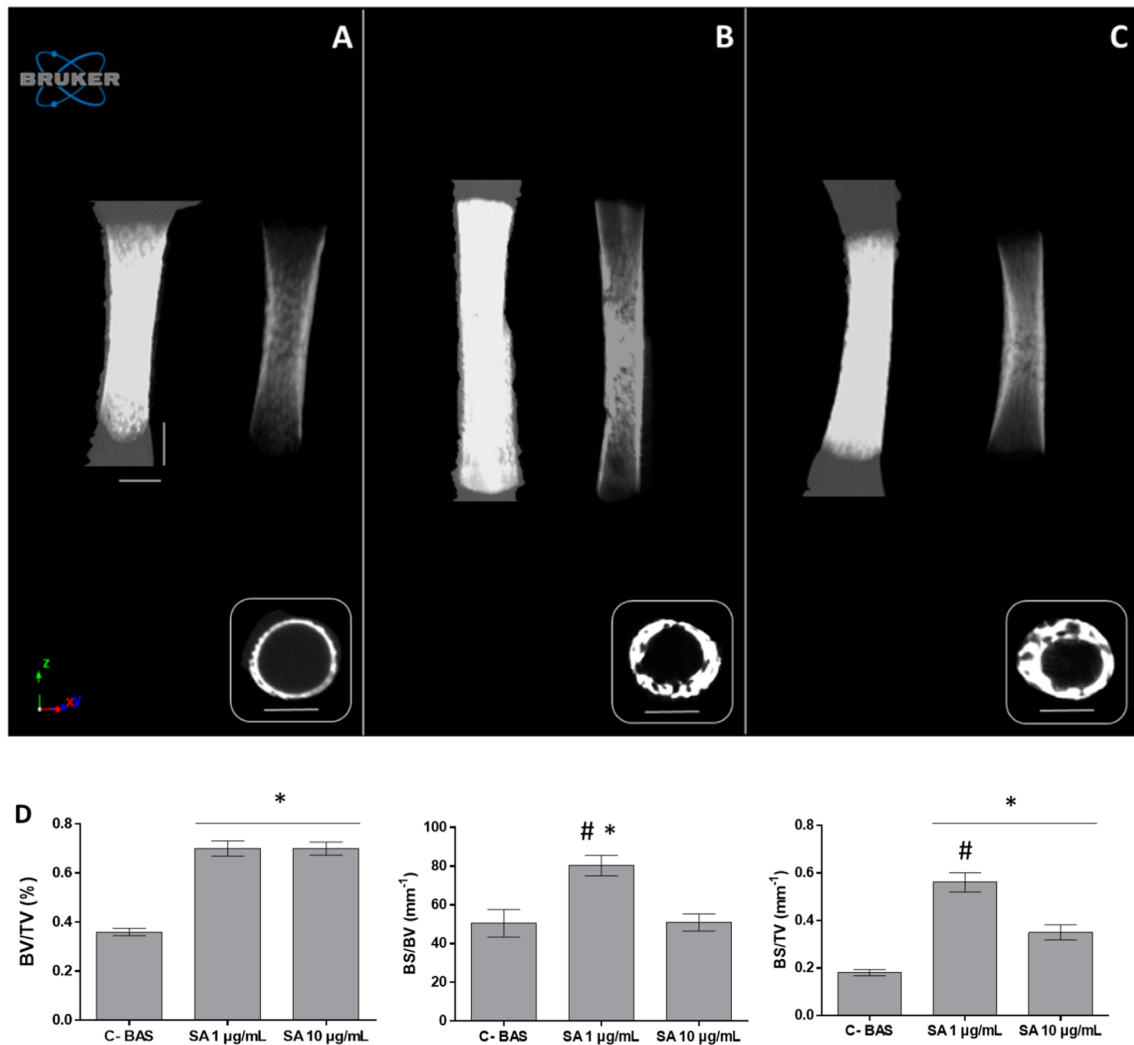
Discussion

In vitro assessment of sarecycline osteogenic functionality

In the present study, hBMSCs were selected as precursor cells to address the osteogenic differentiation potential of SA, given their multilineage differentiation capability, depending partially on external stimuli and condition of culture [17].

Fig. 6 Representative images of µCT analysis. (**A**) C-BAS; (**B**) SA 1 µg/mL; (**C**) SA 10 µg/mL. Images were created setting the defined volume of interest, using the maximum intensity and attenuated projection, respectively. Scale bar corresponds to 500 µm. (**D**) Quanti-tative histomorphometric 3D analysis of the femurs cultured with SA. *Significantly different to control. #Significantly different to SA 10 µg/mL. ($n = 5$, $p < 0.05$). BV, bone volume; BS, bone surface; TV, tissue volume

matrix [29]. Besides, COL1A1, SPARC, and BGLAP genes that encode collagen type I—the main protein component of the osteoid—osteonectin and osteocalcin, respectively—were slightly upregulated or preserved, suggesting the maintenance of the bone matrix production and mineralization, at gene expression level, of cells exposed to SA [30, 31]. The maintenance of osteonectin levels can be observed in the other studies with doxycycline [5]. Furthermore, the downregulation of BMP2 by TCs is documented in the literature, as in the study of Muthukuru and Sun (2013), in which the combination of doxycycline and BMP2 hampered osteogenesis in periodontal ligament cells and in the study of Park [6], wherein three different TCs reduced the expression of BMP2 in osteoprecursor cells [5]. One possible reason for this downregulation may lie on the BMPs' regulation—these

glycoproteins are members of the TGF-β superfamily, known to play an important role regarding inflammation and MMPs' upregulation, via SMADs or other intracellular signals. TCs present anti-inflammatory and a potent anti-MMP activity—therefore, they seem to be able to indirectly decrease BMPs' expression by downregulating the TGF-β signaling and the MMP production [32].

Additionally, SA upregulated the Hedgehog signaling, a key pathway to drive undifferentiated cells to the osteoblast lineage, assessed by GLI2 and PTCH1 gene expression (Fig. 4). GLI2 seems to function as a transcriptional activator when the Hedgehog signaling is active [33], being an essential factor for the endochondral ossification process as, in its absence, a decreased bone formation is attained [34]. Its increased expression seems to upregulate RUNX2, and
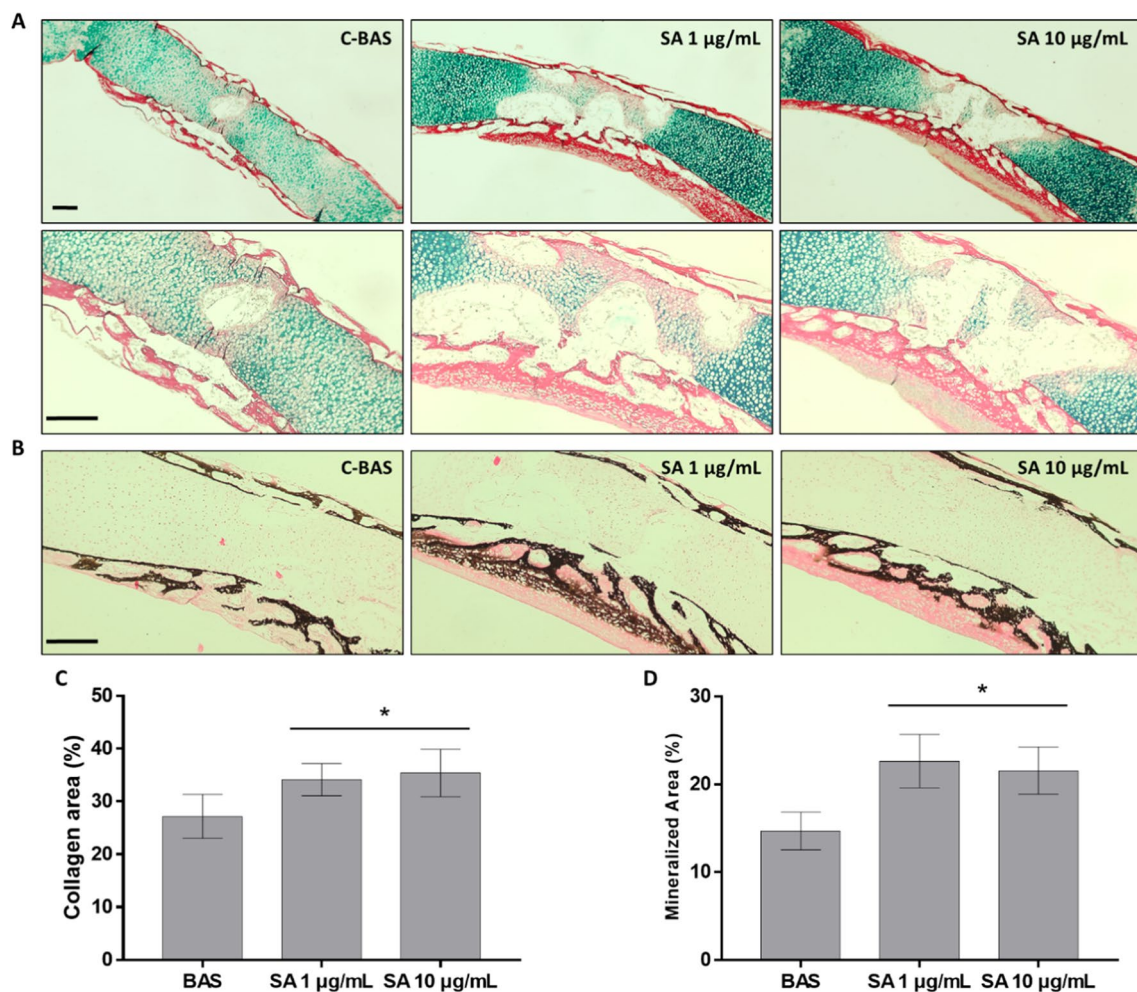
Fig. 7 a Representative images of histochemical staining using Alcian Blue and Sirius Red (AB/SR) staining. Proteoglycans of the cartilage tissue are labeled in blue, while collagen matrix is labeled in red. **b** Representative images of von Kossa staining, with calcium deposits evidenced in black, in addition to a pinkish staining of the cells. **c** Quantitative analysis of the percentage of collagen area using the (AB/SR) stained images. **d** Quantitative analysis of the percentage of mineralized area using von Kossa dyed images. Scale bar corresponds to 100 μm. *Significantly different to control. ($n = 5$, $p < 0.05$)

subsequently the osteogenic activity via a direct physical interaction with the transcription factor [35]. In accordance, RUNX2 expression was found to be significantly increased (Fig. 3), relating to the SA-mediated increase of GLI2.

Notch signaling (assessed via HES and HEY gene expression) is known to be active at early stages of osteoblast differentiation, relying on RUNX2-dependent signaling and known to play a significant role in bone development and repair [28, 36]. HES1 transcription factor is related to an increase of protein stability and transcriptional activity of RUNX2 resulting in the stimulation of osteoblast differentiation [36, 37]. However, the literature seems to be controversial about the timing of HES1 upregulation during osteogenesis, varying from a very early stage of osteoblast differentiation, to a later one [36, 37]. HEY1, on the other hand, seems to inhibit RUNX2 transcriptional activity as

well as bone matrix mineralization, suggesting that HEY1 counteracts RUNX2 and osteoblastic differentiation, at least at early differentiation stages [38]. On the contrary, other studies pointed out that HEY1 is associated with an increased osteogenic differentiation at a late stage, presenting significant increases at day-28 in osteoblastic-precursor cell cultures [36]. In addition, BMP2 is needed for the induction of HEY1 and, as described before, its expression was found to be decreased by SA at the 7-day time point, which could result in the indirect HEY1 downregulation [36, 38].

Finally, little is known about the effects of TCs on Wnt signaling pathway—literature is focused on its carcinogenic potential. The study of Qin et al. [39] doxycycline suppressed the expression of TWIST1 in several cancer cell lines, while tigecycline did not alter AXIN2 expression in cervical squamous cell carcinoma. Moreover, the absence of

HNF1A/TCF1 levels is probably due to the downregulation of the BMP2 gene as previously described, once HNF1A is also related to the BMP/TGF-β signaling pathway and may exist some degree of interdependency between BMPs and HNF1A/TCF1 activity [40]. TWIST1 is a critical modulator of mesenchymal cell fate that induces osteogenic differentiation, while AXIN2 provides a negative feedback on the pathway by promoting the degradation of β-catenin, retarding the osteogenic differentiation [41].

Overall, results suggest that the exposure of hBMSCs to SA enhanced the metabolic activity and the osteogenic differentiation, demonstrated by cell morphology, ALP activity, and gene expression pattern, which showcased the multitude of regulatory pathways that seems to modulate the osteogenic differentiation process [28].

Ex vivo assessment of sarecycline osteogenic functionality: organotypic cultures of embryonic chick femora

The *ex vivo* embryonic chick femora model was chosen to evaluate the effects of SA on the developmental bone growth and mineralization in a more complex biological system. This organotypic culture provides multiple cell types, with a similar organization that is found in in vivo models, allowing the assessment of some intercellular and cell–matrix processes without systemic interferences, easier manipulation, and more ethically acceptable [42].

To the best of our knowledge, it is the first time that a bone development ex vivo system using an air/liquid interface was tested with TCs. However, other types of experiments were performed, as in the study of Cole et al. [43] in which avian tibias were submerged in the presence of doxycycline, and an increase in the length was observed, at 20 and 40 μg/mL, in line with the attained data. Additionally, TCs are usually associated with an improvement in mineralization and bone formation, as presently verified within assessed tissue sections, given the increased collagenous matrix deposition and trabecular mineralization at the mid-diaphysis. For instance, considering in vitro cell models, in the study of Tham et al. [44], the quantification of mineral deposition in BMSCs significantly increased when cells were incubated with nanoparticles loaded with minocycline. Similar results were observed in the study of Muthukuru and Sun [5]—cultures incubated with 1 μg/mL doxycycline presented a significant increase in calcium deposition when compared to control or BMP2 exposure, as in the study of Gomes et al. [45], in which cells treated with 1 μg/mL doxycycline or minocycline increased the extent of matrix mineralization in human osteoblast cultures growing on biomaterials. Regarding in vivo characterization, in the study of Silva et al. [46], a bone cement loaded with minocycline induced a significant higher formation of mineralized tissue, increasing bone outgrown over the surface of the cement and bone-cement contact. As other examples, nanoparticles loaded with tetracycline aiming osteoporosis treatment, a significant increase of the bone mineral density of femurs from ovariectomized rats, as well as nanoparticles loaded with tetracycline conceived to periodontitis treatment significantly increased the percentage of new bone formation in dogs [47].

Conclusions

In the present study, sarecycline stimulated the proliferation and osteogenic differentiation of hBMSCs within in vitro cultures. In addition, for the first time, the relationship of the activation of relevant signaling pathways (i.e., Hedgehog and Notch) and a tetracycline was characterized. Further, an ex vivo embryonic chick femora development model exposed to sarecycline presented an increased collagenous deposition and mineral content, validating the enhanced osteogenesis. These results suggest that sarecycline might be suitable to other medical indications than dermatosis, and is a promising candidate to repurposing for bone tissue-related applications, promoting osteoinduction in a wider concentration' range, in comparison to early generation TCs.

Declarations

Conflict of interest All authors declare that they have no conflict of interest nor financial interests with Adooq Bioscience.

References

1. Weinberg MA, Bral M (1998) Tetracycline and its analogues: a therapeutic paradigm in periodontal diseases. Crit Rev Oral Biol Med 9:322–332. https://doi.org/10.1177/10454411980090030501

2. Garrido-Mesa N, Zarzuelo A, Gálvez J (2013) Minocycline: far beyond an antibiotic. Br J Pharmacol 169:337–352. https://doi.org/10.1111/bph.12139

3. Pushpakom S, Iorio F, Eyers PA, Escott KJ, Hopper S et al (2019) Drug repurposing: progress, challenges and recommendations. Nat Rev Drug Discov 18:41–58. https://doi.org/10.1038/nrd.2018.168

4. Gomes PS, Fernandes MH (2007) Effect of therapeutic levels of doxycycline and minocycline in the proliferation and differentiation of human bone marrow osteoblastic cells. Arch Oral Biol 52:251–259. https://doi.org/10.1016/j.archoralbio.2006.10.005

5. Muthukuru M, Sun J (2013) Doxycycline counteracts bone morphogenic protein 2-induced osteogenic mediators. J Periodontol 84:656–665. https://doi.org/10.1902/jop.2012.120338

6. Park J-B (2011) Effects of doxycycline, minocycline, and tetracycline on cell proliferation, differentiation, and protein expression in osteoprecursor cells. J Craniofac Surg 22:1839–1842. https://doi.org/10.1097/SCS.0b013e31822e8216

7. Suzuki A, Yagisawa J, Kumakura S, Tsutsui T (2006) Effects of minocycline and doxycycline on cell survival and gene expression in human gingival and periodontal ligament cells. J Periodontal Res 41:124–131. https://doi.org/10.1111/j.1600-0765.2005.00843.x

8. Lecio G, Ribeiro FV, Pimentel SP, Reis AA, da Silva RVC et al (2020) Novel 20% doxycycline-loaded PLGA nanospheres as adjunctive therapy in chronic periodontitis in type-2 diabetics: randomized clinical, immune and microbiological trial. Clin Oral Investig 24:1269–1279. https://doi.org/10.1007/s00784-019-03005-9

9. Burgos RM, Rodvold KA (2019) Omadacycline: a novel aminomethylcycline. Infect Drug Resist 12:1895–1915. https://doi.org/10.2147/IDR.S171352

10. Haidari W, Bruinsma R, Cardenas-de-la-Garza JA, Feldman SR (2019) Sarecycline review. Ann Pharmacother 2019:106002801987311. https://doi.org/10.1177/1060028019873111

11. Zhanel G, Critchley I, Lin LY, Alvandi N (2019) Microbiological profile of sarecycline, a novel targeted spectrum tetracycline for the treatment of acne vulgaris. Antimicrob Agents Chemother 63:1–15. https://doi.org/10.1128/AAC.01297-18

12. Bunick CG, Keri J, Tanaka SK, Furey N, Damiani G et al (2021) Antibacterial mechanisms and efficacy of sarecycline in animal models of infection and inflammation. Antibiotics 10:1–12. https://doi.org/10.3390/antibiotics10040439

13. Martin V, Garcia M, Montemor MF, Fernandes JCS, Gomes PS, Fernandes MH (2022) Simulating in vitro the bone healing potential of a degradable and tailored multifunctional mg-based alloy platform. Bioengineering 9:255. https://doi.org/10.3390/bioengineering9060255

14. Garbieri TF, Martin V, dos Santos CF, Gomes PDS, Fernandes MH (2021) The embryonic chick femur organotypic model as a tool to analyze the angiotensin ii axis on bone tissue. Pharmaceuticals 14:469. https://doi.org/10.3390/ph14050469

15. Araújo R, Martin V, Ferreira R, Fernandes MH, Gomes PS (2022) A new ex vivo model of the bone tissue response to the hyperglycemic environment–the embryonic chicken femur organotypic culture in high glucose conditions. Bone 158:116355. https://doi.org/10.1016/j.bone.2022.116355

16. Kanczler JM, Smith EL, Roberts CA, Oreffo ROC (2012) A Novel approach for studying the temporal modulation of embryonic skeletal development using organotypic bone cultures and micro-computed tomography. Tissue Eng Part C Methods 18:747–760. https://doi.org/10.1089/ten.tec.2012.0033

17. Ding DC, Shyu WC, Lin SZ (2011) Mesenchymal stem cells. Cell Transplant 20:5–14. https://doi.org/10.3727/096368910X

18. Shen LC, Chen YK, Lin LM, Shaw SY (2010) Anti-invasion and anti-tumor growth effect of doxycycline treatment for human oral squamous-cell carcinoma—in vitro and in vivo studies. Oral Oncol 46:178–184. https://doi.org/10.1016/j.oraloncology.2009.11.013

19. Onoda T, Ono T, Dhar DK, Yamanoi A, Fujii T, Nagasue N (2004) Doxycycline inhibits cell proliferation and invasive potential: combination therapy with cyclooxygenase-2 inhibitor in human colorectal cancer cells. J Lab Clin Med 143:207–216. https://doi.org/10.1016/j.lab.2003.12.012

20. Garrido-Mesa N, Zarzuelo A, Gálvez J (2013) What is behind the non-antibiotic properties of minocycline? Pharmacol Res 67:18–30. https://doi.org/10.1016/j.phrs.2012.10.006

21. Sagar J, Sales K, Seifalian A, Winslet M (2010) Doxycycline in mitochondrial mediated pathway of apoptosis: a systematic review. Anticancer Agents Med Chem 10:556–563. https://doi.org/10.2174/187152010793498645

22. Chen M, Ona VO, Li M, Ferrante RJ, Fink KB et al (2000) Minocycline inhibits caspase-1 and caspase-3 expression and delays mortality in a transgenic mouse model of Huntington disease. Nat Med 6:797–801. https://doi.org/10.1038/77528

23. Walters B, Uynuk-Ool T, Rothdiener M, Palm J, Hart ML et al (2017) Engineering the geometrical shape of mesenchymal stromal cells through defined cyclic stretch regimens. Sci Rep 7:1–14. https://doi.org/10.1038/s41598-017-06794-9

24. Jhala D, Rather H, Vasita R (2016) Polycaprolactone-chitosan nanofibers influence cell morphology to induce early osteogenic differentiation. Biomater Sci 4:1584–1595. https://doi.org/10.1039/c6bm00492j

25. Almazin SM, Dziak R, Andreana S, Ciancio SG (2009) The effect of doxycycline hyclate, chlorhexidine gluconate, and minocycline hydrochloride on osteoblastic proliferation and differentiation in vitro. J Periodontol 80:999–1005. https://doi.org/10.1902/jop.2009.080574

26. Martin V, Ribeiro IA, Alves MM, Gonçalves L, Claudio RA et al (2019) Engineering a multifunctional 3D-printed PLA-collagen-minocycline-nanoHydroxyapatite scaffold with combined antimicrobial and osteogenic effects for bone regeneration. Mater Sci Eng C 101:15–26. https://doi.org/10.1016/j.msec.2019.03.056

27. Kim Y, Kim J, Lee H, Shin W-R, Lee S et al (2019) Tetracycline analogs inhibit osteoclast differentiation by suppressing MMP-9-mediated histone H3 cleavage. Int J Mol Sci 20:4038. https://doi.org/10.3390/ijms20164038

28. Lattanzi W, Bernardini C (2012) Genes and molecular pathways of the osteogenic process. Osteogenesis. https://doi.org/10.5772/34022

29. Song L (2017) Calcium and bone metabolism indices, vol 82, 1st ed. Elsevier Inc., Hoboken. https://doi.org/10.1016/bs.acc.2017.06.005

30. Rosset EM, Bradshaw AD (2016) SPARC/osteonectin in mineralized tissue. Matrix Biol 52–54:78–87. https://doi.org/10.1016/j.matbio.2016.02.001

31. Hosseini S, Naderi-Manesh H, Vali H, Baghaban Eslaminejad M, Azam Sayahpour F et al (2019) Contribution of osteocalcin-mimetic peptide enhances osteogenic activity and extracellular matrix mineralization of human osteoblast-like cells. Colloids Surfaces B Biointerfaces 173:662–671. https://doi.org/10.1016/j.colsurfb.2018.10.035

32. Santibanez JF, Obradović H, Kukolj T, Krstić J (2018) Transforming growth factor-β, matrix metalloproteinases, and urokinase-type plasminogen activator interaction in the cancer epithelial to mesenchymal transition. Dev Dyn 247:382–395. https://doi.org/10.1002/dvdy.24554

33. Kuwahara ST, Liu S, Chareunsouk A, Serowoky M, Mariani FV (2022) On the horizon: Hedgehog signaling to heal broken bones. Bone Res 10:13. https://doi.org/10.1038/s41413-021-00184-8

34. Miao D, Liu H, Plut P, Niu M, Huo R et al (2004) Impaired endochondral bone development and osteopenia in Gli2-deficient mice. Exp Cell Res 294:210–222. https://doi.org/10.1016/j.yexcr.2003.10.021

35. Shimoyama A, Wada M, Ikeda F, Hata K, Matsubara T et al (2007) Ihh/Gli2 signaling promotes osteoblast differentiation by regulating Runx2 expression and function. Mol Biol Cell 18:2411–2418. https://doi.org/10.1091/mbc.e06-08-0743

36. Bagheri L, Pellati A, Rizzo P, Aquila G, Massari L et al (2018) Notch pathway is active during osteogenic differentiation of human bone marrow mesenchymal stem cells induced by pulsed electromagnetic fields. J Tissue Eng Regen Med 12:304–315. https://doi.org/10.1002/term.2455

37. Suh JH, Lee HW, Lee JW, Kim JB (2008) Hes1 stimulates transcriptional activity of Runx2 by increasing protein stabilization during osteoblast differentiation. Biochem Biophys Res Commun 367:97–102. https://doi.org/10.1016/j.bbrc.2007.12.100

38. Zamurovic N, Cappellen D, Rohner D, Susa M (2004) Coordinated activation of Notch, Wnt, and transforming growth factor-β signaling pathways in bone morphogenic protein 2-induced osteogenesis: Notch target gene Hey1 inhibits mineralization and Runx2 transcriptional activity. J Biol Chem 279:37704–37715. https://doi.org/10.1074/jbc.M403813200

39. Qin Y, Zhang Q, Lee S, Zhong WL, Liu YR et al (2015) Doxycycline reverses epithelial-to-mesenchymal transition and suppresses the proliferation and metastasis of lung cancer cells. Oncotarget 6:4066779. https://doi.org/10.18632/oncotarget.5842

40. Bonner C, Farrelly AM, Concannon CG, Dussmann H, Baquie M et al (2011) Bone morphogenetic protein 3 controls insulin gene expression and is down-regulated in INS-1 cells inducibly expressing a hepatocyte nuclear factor 1A-maturity-onset diabetes of the young mutation. J Biol Chem 286:25719–25728. https://doi.org/10.1074/jbc.M110.215525

41. Di Pietro L, Barba M, Prampolini C, Ceccariglia S, Frassanito P et al (2020) Gli1 and axin2 are distinctive markers of human calvarial mesenchymal stromal cells in nonsyndromic craniosynostosis. Int J Mol Sci 21:1–19. https://doi.org/10.3390/ijms21124356

42. Smith E, Kanczler J, Oreffo R (2013) A new take on an old story: chick limb organ culture for skeletal niche development and regenerative medicine evaluation. Eur Cells Mater 26:91–106. https://doi.org/10.22203/eCM.v026a07

43. Cole AA, Chubinskaya S, Luchene LJ, Chlebek K, Orth MW et al (1994) Doxycycline disrupts chondrocyte differentiation and inhibits cartilage matrix degradation. Arthritis Rheum 37:1727–1734. https://doi.org/10.1002/art.1780371204

44. Tham AY, Gandhimathi C, Praveena J, Venugopal JR, Ramakrishna S, Kumar SD (2016) Minocycline loaded hybrid composites nanoparticles for mesenchymal stem cells differentiation into osteogenesis. Int J Mol Sci 17:1–16. https://doi.org/10.3390/ijms17081222

45. Gomes PS, Santos JD, Fernandes MH (2008) Cell-induced response by tetracyclines on human bone marrow colonized hydroxyapatite and Bonelike®. Acta Biomater 4:630–637. https://doi.org/10.1016/j.actbio.2007.12.006

46. Silva T, Silva JC, Colaco B, Gama A, Duarte-Araújo M et al (2018) In vivo tissue response and antibacterial efficacy of minocycline delivery system based on polymethylmethacrylate bone cement. J Biomater Appl 33:380–391. https://doi.org/10.1177/0885328218795290

47. Lee BS, Lee CC, Wang YP, Chen HJ, Lai CH et al (2016) Controlled-release of tetracycline and lovastatin by poly(D, L-lactide-co-glycolide acid)-chitosan nanoparticles enhances periodontal regeneration in dogs. Int J Nanomed 11:285–297. https://doi.org/10.2147/IJN.S94270